

# Recurrence-time statistics in non-Hamiltonian volume preserving maps and flows

Rafael M. da Silva<sup>1,2,\*</sup>, Marcus W. Beims<sup>1,2,†</sup> and Cesar Manchein<sup>1‡</sup>

<sup>1</sup>*Departamento de Física, Universidade do Estado de Santa Catarina, 89219-710 Joinville, Brazil and*

<sup>2</sup>*Departamento de Física, Universidade Federal do Paraná, Caixa Postal 19044, 81531-980 Curitiba, Brazil*

(Dated: 16 de outubro de 2018)

We analyze the recurrence-time statistics (RTS) in three-dimensional non-Hamiltonian volume preserving systems (VPS): an extended standard map, and a fluid model. The extended map is a standard map weakly coupled to an extra-dimension which contains a deterministic regular, mixed (regular and chaotic) or chaotic motion. The extra-dimension strongly enhances the trapping times inducing plateaus and distinct algebraic and exponential decays in the RTS plots. The combined analysis of the RTS with the classification of ordered and chaotic regimes and scaling properties, allows us to describe the intricate way trajectories penetrate the before impenetrable regular islands from the uncoupled case. Essentially the plateaus found in the RTS are related to trajectories that stay long times inside trapping tubes, not allowing recurrences, and then penetrates diffusively the islands (from the uncoupled case) by a diffusive motion along such tubes in the extra-dimension. All asymptotic exponential decays for the RTS are related to an ordered regime (quasi-regular motion) and a mixing dynamics is conjectured for the model. These results are compared to the RTS of the standard map with dissipation or noise, showing the peculiarities obtained by using three-dimensional VPS. We also analyze the RTS for a fluid model and show remarkable similarities to the RTS in the extended standard map problem.

PACS numbers: 05.45.Jn, 05.45.Pq, 05.45.Ra

## I. INTRODUCTION

The seminal work of Henri Poincaré brought up to attention a very important fact: the motion of an incompressible fluid of finite volume is recurrent [1]. For Hamiltonian systems this means that almost all orbits come arbitrarily close to an initial point an infinite number of times. For many years the properties of such recurrences have been analyzed in distinct physical situations by using the RTS. It was observed that the RTS is capable of describing the relevant aspects of the dynamics in complex systems. In this context, we mention that the RTS is able to describe universal algebraic decays in Hamiltonian systems [2–4], including random walk penetration of the Kolmogorov-Arnold-Moser (KAM) islands [5, 6], biased random walk to escape from KAM island [7], DNA sequence [8], synchronization of oscillator [9], generalized bifurcation diagram of conservative systems [10], fine structure of resonance islands [11], transient chaos in systems with leaks [12], among others.

In distinction to the above works related to area-preserving maps, a novel situation occurs for non-Hamiltonian three-dimensional (3D) VPS, whose dynamics has applications in volume-preserving flows, and chaotic scattering, where particles are captured and scattered on resonance (see Ref. [13] for a detailed discussion). One work in this direction related the RTS with anomalous transport in a fluid flow [14]. In case of scattering problems, there exist a scattering region where

interactions between particles and the system of interest occur. Outside this region the action of the system is insignificant so that the particles motion is not of relevance. Essential properties from the system of interest is revealed from the behavior of the scattered particles. In fact, scattering is one of the fundamental tools to unveil the main characteristics of processes in nature, such as in chemical reactions, atomic and nuclear physics, fluid and celestial mechanics [15–17]. Recent attentions focused on scattering in conservative systems, where regular and chaotic dynamics coexist and particles can be trapped for finite times close to regular islands leading to an algebraic temporal decay of the scattered particles, which perform a transient chaotic motion. In realistic experiments, the scattered particles may also be subjected to noise, dissipation, external forces, etc. In most cases noise destroys the KAM curves and the algebraic decay is replaced by the exponential [18–20], or stretched exponential [21]. However, recent developments have shown that noise can enhance the algebraic decay due to trajectories performing a random walk motion inside the KAM islands [5, 6]. Biased random walk was also observed in the standard map under random symplectic perturbations [7].

On the other hand, flows in three-dimensions arise in a number of different applied contexts such as fluid dynamics and transport of matter in a fluid [22–24]. Nonlinear maps can be obtained from fluid flow models and are of two types: action-action-angle and action-angle-angle maps. Whereas a action-angle-angle volume-preserving map is analogous to symplectic maps when it comes to KAM theorem, the behavior of action-action-angle maps is very different. It was shown [25] that no invariant 2D surfaces persist upon perturbation from an integrable action-action-angle map and at these same locations

\* rmarques@fisica.ufpr.br

† mbeims@fisica.ufpr.br

‡ cesar.manchein@udesc.br

in the phase-space periodic orbits of specific type persist and they dominate the transport in the perturbed map. Besides, many initial conditions can create trajectories that go through a large portion of the phase-space even when the map is very close to being integrable. This has been named *resonance-induced dispersion* (RID) [26–28].

In this work we analyzed the RTS for two systems: First an action-action-angle map, called the Extended Standard Map (*ESM*), introduced in Sec. II, a non-Hamiltonian 3D VPS which can be associated with the chaotic scattering problem mentioned above. Our discussion will be mainly focused in the (*ESM*) system. Secondly we consider a fluid flow model [23] to show the astonishing similarities to the RTS in the *ESM*. For the case of the 3D non-Hamiltonian map considered (the *ESM*), we use an additional deterministic dimension, weakly coupled to the standard map (vortices in the fluid case), which allows particles to penetrate the regular islands from the uncoupled case, and eventually approach the center of the island. Mainly we show that the extra-dimension strongly enhances the trapping time around the regular island from the standard map (vortices), resulting in plateaus (not allowing recurrences) and algebraic decays in the characteristics recurrence curves and generating asymptotic exponential decays as typically observed, for instance, in area-preserving maps. While short time exponential and long time algebraic decays are similar to those found in Hamiltonian system, the large plateaus are apparently a particular property of 3D VPS. We mention here that the plateaus were also found in a totally distinct context, a fertility model which has some applications to earthquakes [29]. In addition, asymptotic exponential decays appear to be common in 3D VPS. In our analysis we combine the RTS and a recent developed technique [30], which uses finite-time Lyapunov exponents (FTLEs), to efficiently determine the time evolution of ordered (**O**), and chaotic (**C**) regimes. This allows us to clearly associate the decays of cumulative distribution of consecutive time spent in the regime **O** (algebraic or exponential), with the penetration inside the regular islands from the uncoupled case. Scalings properties of the RTS show that the physical origin of the asymptotic decays is the same for different small couplings intensities with the extra-dimension.

Finally, with this work we also intend to give some insight about possible answer for the following questions: “Do recurrence-time distributions in typical volume-preserving maps with regular and chaotic components have an asymptotic power-law form like Hamiltonian systems with mixed dynamics? Is there an universal decay exponent of recurrences? Similar questions were proposed recently [31], where the author summarizes both, the

state of the art in the theory of transport for conservative dynamical systems, based on the last thirty years of investigations, and tries to point out some open problems that could be addressed next.

This work is organized in the following manner. While Sec. II presents the three-dimensional volume preserving model used to describe our results, Sec. III briefly describes the methods of the RTS and classification of regimes using the time dependent finite-time Lyapunov spectrum. In Sec. IV the results for the *ESM* are discussed, and are compared to the standard map with dissipation or noise in Sec. V. Section VI discusses the results for the fluid flow model and concluding remarks are summarized in Sec. VII.

## II. THE COUPLED MAPS MODEL

Our main benchmark tool in this work is the *ESM* defined by

$$\begin{cases} p_{n+1} = p_n + \frac{K_1}{2\pi} \sin(2\pi x_n) + \frac{\delta}{2\pi} \sin(2\pi w_n) \mod 1, \\ w_{n+1} = w_n + \frac{K_2}{2\pi} \sin(2\pi x_n) \mod 1, \\ x_{n+1} = x_n + p_{n+1} \mod 1, \end{cases} \quad (1)$$

where the parameter  $K_1$  determines the dynamics of the area-preserving standard map, the parameter  $K_2$  establishes the dynamics of the extra-dimension as regular, mixed or chaotic, and the parameter  $\delta$  is a measure of the intensity of the coupling between the standard map and the extra-dimension. Some analytic properties of this model are investigated in Ref. [28].

For  $\delta = 0$ , the map given by Eq. (1) reduces to the usual standard map in  $x$  and  $p$  coordinates, while  $w$  behaves like another action coordinate [32]. The standard map has a well known rich dynamics [15, 33], which changes from regular for small  $K_1$ , to mixed for intermediate values of  $K_1$  or to totally chaotic for large  $K_1$ . For clarity, in Fig. 1 we plot the phase-space of the standard map for the uncoupled case, showing the (a) regular dynamics, (b) and (c) the mixed dynamics, and (d) the chaotic dynamics. The coupled dynamics for  $\delta > 0$  intermixes the motions observed in Fig. 1 and the resulting regular structure in 3D phase-space can have a complicated shape. To be precise with the terminology, for the uncoupled case we will use *regular island* (which cannot be penetrated), while for the coupled case we use *regular structure* (which can be penetrated).

---

A stability analysis, not presented here, shows that the stable period-1 and 4 resonances shown in Fig. 1 become

---

unstable for  $\delta > 0$ . Therefore, the center of the regular structure becomes unstable and has crucial consequences

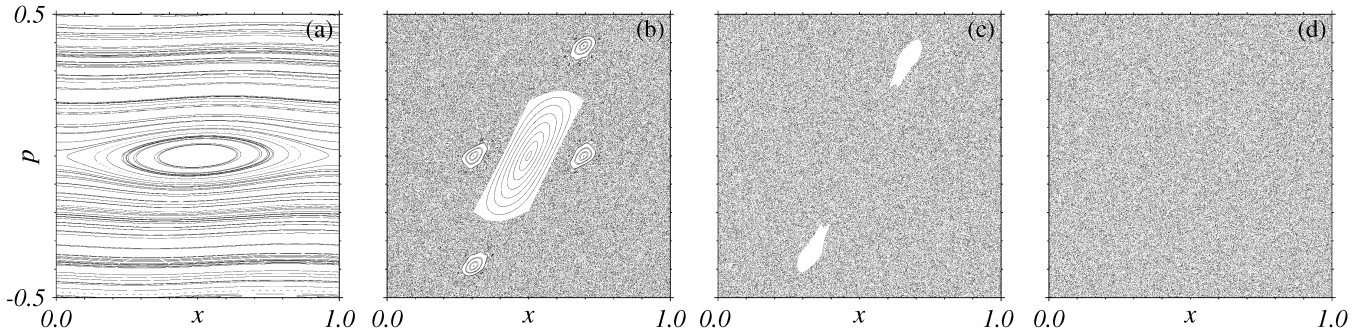


Figure 1. Phase-space dynamics of the uncoupled ( $\delta = 0$ ) standard map using (a)  $K_1 = 0.09$  (regular dynamics), (b)  $K_1 = 2.6$  (mixed dynamics), (c)  $K_1 = 4.9$  (mixed dynamics) and (d)  $K_1 = 8.8$  (chaotic dynamics). These values will define the dynamics of the extra-dimension coupled to the standard map (see Sec. IV). Here we used 80 randomly equally distributed ICs and  $3 \times 10^4$  iterations for each IC.

for our results. There might exist other regular structures with stable centers for this model, but we have not found them. In fact, other kind of couplings and/or extra-dimension dynamics could be used to keep the stability of the center of the structure, but this will certainly change the results presented in Sec. IV.

### III. METHODS

Two methods, or techniques, will be used to carefully describe the influence of the extra-dimension on the scattered trajectories, as briefly discussed in the Sec. I.

#### A. Recurrence-time statistics

The first technique is the RTS determined numerically by computing the quantity of iterations  $\tau$  that the trajectory, starting from an initial pre-delimited chaotic region, collides with the regular structure and comes back to the initial region, called recurrence region. We are interested in the cumulative probability distribution  $P_{cum}(\tau)$  defined by

$$P_{cum}(\tau) \equiv \sum_{\tau'=\tau}^{\infty} P(\tau'), \quad (2)$$

that gives essential informations about the presence, or not, of sticky motion in conservative systems. Straight lines in the log-log plot of this distribution are power-law decays of the form  $P_{cum}(\tau) \propto \tau^{-\gamma}$ , where  $\gamma$  is the decay exponent. Such decays are usually related to sticky effects induced by the invariant structures on the chaotic trajectory [4]. To reckon  $P_{cum}(\tau)$  we always start with ICs randomly distributed inside the recurrence region defined by  $-0.2 \leq x \leq 0.2$ ,  $0.5 \leq p \leq 0.5$  and  $-0.5 \leq \omega \leq 0.5$ . Each time the recurrence region is mentioned, it means that the trajectory is already ejected from the region close to the regular structure. We

also tested other boxes for the recurrence region, with different sizes, but our main results remain unchanged.

#### B. Lyapunov Regimes

The second technique consists in using the FTLEs spectrum  $\{\lambda_i^{(\Omega)}\}$  to classify ordered and chaotic regimes in time as proposed recently [30]. For the *ESM* model we have three FTLEs ( $i = 1, 2, 3$ ) which satisfy  $\lambda_3^{(\Omega)} = -\lambda_1^{(\Omega)}$  and  $\lambda_2^{(\Omega)} = 0$ . In order to implement this technique, we follow a trajectory and compute the FTLEs spectrum during a window of size  $\Omega$ , and explore the temporal properties in the time series of  $\lambda_1^{(\Omega)}$ . Starting with a typical initial condition chosen in a chaotic region where the largest FTLE is greater than zero, we follow the trajectory and for times  $t = m\Omega$  ( $m = 1, 2, \dots, N$ ) we evaluate  $\lambda_1^{(\Omega)}$ . If this trajectory is close to the regular structure we have  $\lambda_1^{(\Omega)} \approx 0.0$ . This allows us to classify distinct regimes as *ordered O*, for  $\lambda_1^{(\Omega)} \approx 0$ , and *chaotic C*, for  $\lambda_1^{(\Omega)} > 0$ , as exemplified in Fig. 2 along a time series of  $\lambda_1^{(100)}$ . In the regime *O* the trajectory is close to the regular structure and for regime *C* it is in the chaotic region of the phase space. From this analysis we can obtain the cumulative probability distribution defined as

$$P_{cum}(\tau_M) \equiv \sum_{\tau'_M=\tau_M}^{\infty} P(\tau'_M), \quad (3)$$

where  $\tau_M$  is the time spent consecutively in one of the two possible regimes and  $M = \mathbf{O}, \mathbf{C}$  indicates the corresponding regime. It is worth to mention that the ordered regime is composed by a chaotic trajectory which moves, for a finite-time, close to a regular island (sticky motion). It has been shown [30] that this classification of regimes significantly improves the ability of the stickiness characterization and, by associating them with the distinct decays in the RTS, a clear picture of the underlying dynamics.

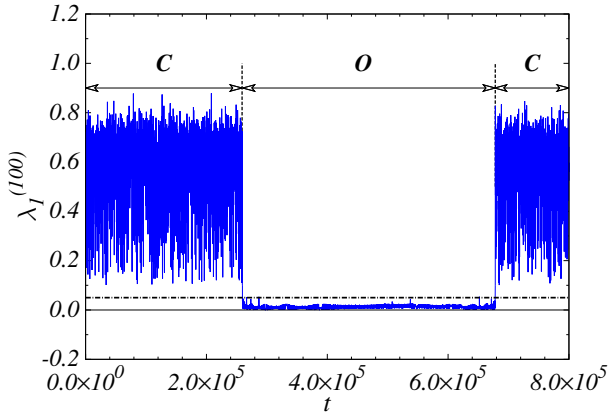


Figure 2. (Color online) Illustration of the method used to define the regimes **O** and **C**. The time series of the FTLE  $\lambda_1^{(\Omega=100)}$  for the *ESM* is plotted. The threshold  $\varepsilon = 0.05$  that defines the regimes is plotted by a dashed-dotted line. A typical initial condition used to generate this time series was chosen inside the chaotic sea.

#### IV. RESULTS

In this Section the numerical results are analyzed. For all simulations we use a mixed dynamics ( $K_1 = 2.6$ ) for the standard map, and change the dynamics of the extra-dimension using the following values  $K_2 = 0.09, 2.6, 4.9$  and  $8.8$  (see Fig. 1).

##### A. Recurrence-time statistics plots

Figure 3 (a)-(d) displays the log-log plot of the RTS as a function of  $\tau$  for different values of  $K_2$ . For comparison we show the uncoupled standard map case  $\delta = 0$  (black-dashed line), which displays an exponential decay for small times followed by the power law decay ( $\sim \tau^{-1.62}$ ) due to sticky effects. For all couplings we still have the power-law decay ( $\sim \tau^{-1.62}$ ) for shorter times. After these times, a plateau is seen whose width depends on the coupling strength. The plateau in the RTS means that no recurrences were observed for these times. As will be shown later, during the plateaus the trajectory moves around the regular islands from the uncoupled case and do not return to the recurrence region. For increasing values of the coupling, we observe that the plateaus appear for earlier times and become shorter. This occurs independently of the dynamics in the extra-dimension,

but tend to disappear for  $\delta \sim 10^{-1}$  (not shown here) in the regular case in Fig. 3(a), and for  $\delta \sim 10^{-3}$  (cyan-dashed-dotted line) in the mixed and chaotic cases shown in Figs. 3(b)-(d). Besides the mixed case from Fig. 3(c), which has an abrupt break of the plateau, where all plateaus are followed by exponential decays for larger times. In fact, the case  $\delta \sim 10^{-3}$  in Fig. 3(c) also shows the asymptotic exponential decay after the abrupt break of the plateau and a smooth power law related with the random walk performed by the trajectory inside the regular structures. In general we observe the following decays:

- **C**: Exponential decay for very short times (not discussed in this work).
- **O<sub>1</sub>**: Power-law with  $P_{cum}(\tau) \propto \tau^{-1.62}$  for  $\tau < \tau_{p_\delta}$ , where  $\tau_{p_\delta}$  is the time when the plateau appears for given  $\delta$ . This decay is the only one (besides **C**) observed for  $\delta = 0$ , and the first one (after **C**) observed for all analyzed couplings.
- **O<sub>2</sub>**: Plateaus obeying  $P_{cum}(\tau) \propto \delta$  for times  $\tau_{p_\delta} < \tau < \tau_{p'_\delta}$ , where  $\tau_{p'_\delta}$  is the time where the plateaus disappear.

After the plateaus we see distinct behaviors which depend on the dynamics of the extra-dimension:

- **O<sub>3</sub>**: An exponential decay with  $P_{cum}(\tau) \propto e^{-\eta\tau}$  for  $\tau > \tau_{p'_\delta}$ . This is the asymptotic behavior for the cases  $K_2 = 0.09$  in Figs. 3(a),(e),(i), and  $K_2 = 8.8$  in Figs. 3(d),(h), (l), and intermediate decay for  $K_2 = 2.6$  in Figs. 3(b),(f) and (j).
- **O'<sub>3</sub>**: An asymptotic exponential decay with  $P_{cum}(\tau) \propto e^{-\eta\tau}$ , only observed in Figs. 3(b),(f) and (j), when using  $K_2 = 2.6$ .
- **O<sub>4</sub>**: A short power-law with  $P_{cum}(\tau) \propto \tau^{-4.6}$  after the abrupt break of the plateau. This was only observed for  $K_2 = 4.9$  in Figs. 3(c),(g) and (k). Other simulations (not presented here) also show the abrupt break of the plateau for values close to  $K_2 \sim 4.9$ .
- **O<sub>5</sub>**: After **O<sub>4</sub>** a random walk with  $P_{cum}(\tau) \propto \tau^{-0.5}$  occurs (also only for  $K_2 = 4.9$ ).

These distinct behaviors of the RTS in the ordered regime can be better visualized in the insets of Figs. 3(a)-(d). Before discussing in details the physical origin of the decays, we equip ourselves with the regimes technique, introduced in the Sec. IIIB, to have a better understanding of the underline dynamics.

##### B. Regimes of ordered and chaotic motion

Using the classification of regimes it is possible to recognize the dynamics for the different decays. This is

shown in Fig. 3(e)-(h) for only one coupling strength ( $\delta = 10^{-5}$ ), which was chosen because it contains all

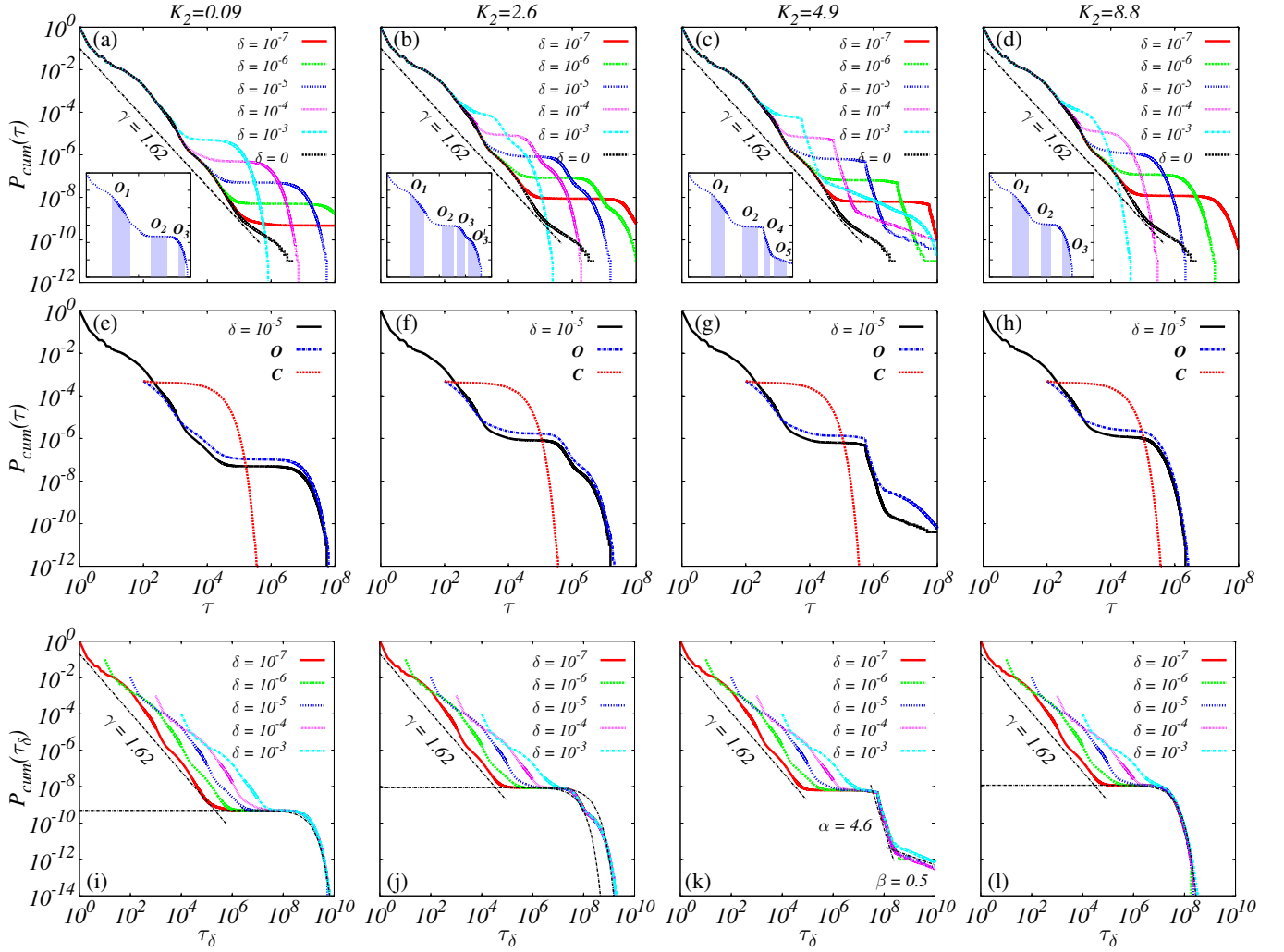


Figure 3. (Color online) In top and bottom lines are plotted the cumulative probability distributions  $P_{cum}(\tau)$  [Eq. (2)] for recurrence-times  $\tau$  and its scaled version  $P_{cum}(\tau_\delta)$  [Eq. (4)] respectively, for different values of the coupling  $\delta$ . For  $\delta = 0$  we recover results for the standard map. For clarity, the insets in the top line show the distinct behaviors ( $\mathbf{O}_1, \mathbf{O}_2, \mathbf{O}_3, \dots$ ) of the RTS in the ordered regime for  $\delta = 10^{-5}$ . In the middle line we also plot  $P_{cum}(\tau)$  for recurrence-times  $\tau$  (black-continuous lines) together with  $P_{cum}(\tau = \tau_M \Omega)$  [Eq. (3)] for the regimes  $\mathbf{C}$  (red-dashed lines) and  $\mathbf{O}$  (blue-dashed-dotted lines) for  $\delta = 10^{-5}$ . Different values of  $K_2$  are used, namely  $K_2 = 0.09$  (regular dynamics) in (a),(e),(i);  $K_2 = 2.6$  (mixed dynamics) in (b),(f),(j);  $K_2 = 4.9$  (mixed dynamics) in (c),(g),(k) and  $K_2 = 8.8$  (chaotic dynamics) in (d),(h),(l). In all simulations we used  $\Omega = 100$ .

distinct decays we have found. In fact, the scaling properties presented in next Section shows that the relevant dynamics is not coupling dependent in the limit of small couplings. The chaotic regime  $\mathbf{C}$  is connected to the exponential decay for smaller times (not shown in details). The ordered regime astonishingly reproduces the power-law decays ( $\mathbf{O}_1$ ), plateaus ( $\mathbf{O}_2$ ), plateaus break ( $\mathbf{O}_4$ ), and the asymptotic exponential decay ( $\mathbf{O}_3, \mathbf{O}_{3'}$ ), and the random walk ( $\mathbf{O}_5$ ). Additional simulations (not shown) realized for other values of  $\delta$ , also reveal the connection between chaotic regime  $\mathbf{C}$  to the exponential decay for smaller times, and the ordered regime  $\mathbf{O}$  to all later decays.

### C. Scaling

From the top line of Fig. 3 we observe that, for a given  $K_2$ , curves with different  $\delta$  are superposed in the exponential ( $\mathbf{C}$ ) and power-law decay ( $\mathbf{O}_1$ ) for short times. Only for intermediate and larger times they start to separate from each other. For these times the RTS follows the scaling

$$\tau_\delta = \frac{\delta'}{\delta} \tau_{\delta'}, \quad P_{cum}(\tau_\delta) = \frac{\delta}{\delta'} P_{cum}(\tau_{\delta'}), \quad (4)$$

where  $\tau_\delta$  ( $\tau_{\delta'}$ ) is the recurrence-time for a given coupling strength  $\delta$  ( $\delta'$ ). This scaling is shown in the bottom line of Fig. 3. The time where the plateaus disappear are now exactly the same, independent of the couplings (for

small couplings). The same scaling occurs in Fig. 3(k), where the abrupt break of the plateau and the random walk occurs. This shows that larger couplings strongly anticipate the asymptotic decay of the RTS. Moreover, it is possible to describe the decays of the RTS by the expression

$$P_{cum}(\tau) \sim (a\tau^{-\gamma} + b\nu)e^{-c\nu\tau}, \quad (5)$$

where  $a, b$  are constants to be determined and  $\nu = 10^{-2}\delta$ . Additionally, in Fig. 4 we show that the intervals for which the plateaus exist  $\Delta\tau$ , has an inverse dependence on  $\delta$ , *i. e.*  $\Delta\tau \propto (1/\delta)^{1.05}$ . This result is almost independent of the regular, mixed or chaotic dynamics of the extra-dimension.

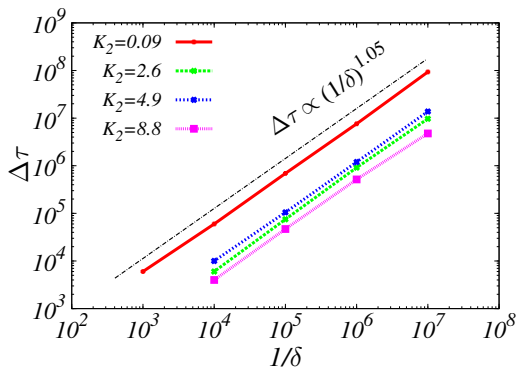


Figure 4. (Color online) Time interval  $\Delta\tau = \tau_{p'_\delta} - \tau_{p_\delta}$  where the plateaus exist has a function of the inverse of the coupling strength. These times were obtained from the recurrences curves of Fig.3(a)-(d).

#### D. Diffusion channels and the penetration of islands

Here we show the dynamics in the 2D projection in the variables  $(x, p)$  and the 3D phase-spaces for specific times, where the RTS has distinct decays. This allows us to clearly understand the dynamics that occurs at the decays, plateaus, abrupt break of the plateaus, random

walk and the asymptotic exponential decay. It also shows how trajectories use the extra-dimension to penetrate the island.

The 2D phase-spaces (projections of the dynamics in 3D) are shown in Fig. 5, with colors indicating the points plotted during the different time decays, as shown in the insets of the figures. The power-law decays for times  $\mathbf{O}_1$  are associated to the sticky motion around (but outside) the regular structures. The plateaus ( $\mathbf{O}_2$ ) in the RTS are related to points in the phase-space where the trajectory remains close to the border (but inside) of the structures. This occurs also close to higher-order resonances, better visualized in Figs. 5(a),(c) and (d). In the corresponding 3D plots displayed in Fig. 6, we observe that for times where the plateaus exist, the chaotic trajectory is mainly trapped to the regular structure, but deep into the extra-dimension  $w$ . The trajectory performs a spiralling motion along the  $w$  direction, leading to the green trapping tube, which can be better recognized in Figs. 6(a),(c) and (d). After the plateaus, exponential decays  $\mathbf{O}_3$  occur in Fig.5(a),(b) and (d) which are related to the penetration of the trajectory in the regular structures, going towards the center. Exception is the penetration of the period-1 large structure in Fig. 5(d). From Figs. 6(a) and (b) we can better see that the motions towards the center of the regular structures occur via the extra-dimension, repeating the motion along the trapping tube with a smaller radius. As mentioned before, the stable period-1 and 4 resonances become unstable for  $\delta > 0$ . Therefore, they act as resonances which eject the trajectories along the trapping tube in the extra-dimension, a process which remembers the RID. An interesting break of the central structure is observed in the  $w$  coordinates, due the high-perturbation caused by the extra-dimension, which inhibits the penetration of this structure. The additional  $\mathbf{O}_3$  exponential behavior occurs only in Fig. 5(b), and is solely related to the penetration of the higher-order resonances period-4 islands from the uncoupled case. This is also nicely confirmed in Fig. 6(b). The short time superdiffusive decay  $\mathbf{O}_4$  in Fig. 5(c) is also related to the penetration of the regular structures, but the injection via the tube in the extra-dimension is clearly distinct, as seen in Fig. 6(c), from which we conclude that the trajectory first reach the center of the period-4 and period-1 structures, and after that it is ejected along the tubes.

The last observed power-law decay,  $\mathbf{O}_5$ , occurs only inside the main regular structure and is related to a random walk motion restricted to the boundaries imposed by the regular structure. This occurs just for finite times and we expect an exponential decay for larger times (not shown), as nicely discussed in [5] for the case of noise. Amazingly, all the dynamics shown in Figs. 5 and 6 are related to the approximated regular motion which belongs to the regime  $\mathbf{O}$ . Even the asymptotic exponential

decays of the RTS are related to this regime and suggest the mixing nature of the dynamics [5].

#### V. UNCOUPLED CASE WITH DISSIPATION OR NOISE

In this Section we compare our results of a deterministic perturbation in the standard map to other kind of



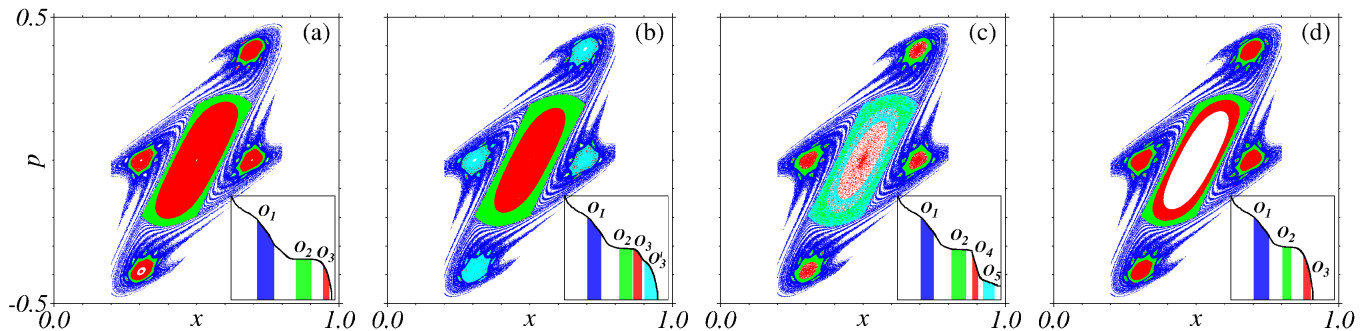


Figure 5. (Color online) Phase-space projected in  $(x, p)$  for  $\delta = 10^{-5}$  and (a)  $K_2 = 0.09$  (regular dynamics) (b)  $K_2 = 2.6$  (mixed dynamics) (c)  $K_2 = 4.9$  (mixed dynamics) and (d)  $K_2 = 8.8$  (chaotic dynamics). The insets show the RTS, the same insets from the top line of Fig. 3, but now with colors indicating the different time intervals  $\mathbf{O}_1, \mathbf{O}_2, \mathbf{O}_3, \mathbf{O}'_3, \mathbf{O}_4$  and  $\mathbf{O}_5$ , for which the corresponding phase-space points were plotted with the same color.

perturbations. It has been argued that noise and dissipation can play the role of an extra-dimensional environment. Therefore we are now interested in comparing the RTS from our extra deterministic dimension with the RTS by using noise or dissipative extra-dimensions. With this purpose in mind we take the following map

$$\begin{cases} p_{n+1} = \left(1 - \frac{\gamma_S}{2\pi}\right) p_n + \frac{K}{2\pi} \sin(2\pi x_n) + \frac{D}{2\pi} \xi_n, \\ x_{n+1} = x_n + p_{n+1}, \end{cases} \quad (6)$$

which is the standard map with dissipation and noise. The dissipation constant is  $0 \leq \gamma_S \leq 1$  and  $\xi_n$  is the white noise, equally distributed in the interval  $[-1, 1]$ , with intensity  $D/2\pi$ . The standard map close to the conservative limit has a larger number of resonances ( $\sim 1/\gamma_S$ ) which essentially determine the kind of dynamics. All regular trajectories surrounding the resonances will converge asymptotically to the center of the stable islands. The effect of dissipation on the RTS with  $D = 0$  is shown in Fig. 7(a), demonstrating that dissipation induces plateaus which remain for all the iterated times. In other words, the chaotic trajectory only returns to the recurrence region for smaller times. For larger times it is attracted by the elliptic points from the conservative case which were transformed into sinks due to the dissipation. Thus plateaus are related to trajectories which converge to the sinks and never return. The times  $\tau_{\gamma_S}$  and  $\tau'_{\gamma'_S}$  for which the plateaus appear for different dissipation parameters  $\gamma_S$  and  $\gamma'_S$  are scaled by

$$\tau_{\gamma_S} = \frac{\gamma_S}{\gamma'_S} \tau'_{\gamma'_S} \quad (7)$$

and are therefore proportional to the number of resonances. This confirms that the plateaus observed in Sec. IV are also related to the penetration of the island. However, in that case the center of the regular structure are unstable points and eject the trajectory back to the recurrence region via the extra-dimension. Thus, to return to the recurrence region the trajectory needs to reach the

center of the structure and, therefore, the plateau times observed in Sec. IV are the times the trajectory need to penetrate the regular structure. These times are proportional to  $\sim 1/\delta$ .

Figure 7(b) displays the RTS for the case of noise with  $\gamma_S = 0$ . Small noise intensities induce an enhanced power-law decay which tend to disappear for larger values of  $D$ . For  $D = 10^{-3}$  we observe that, in addition to the power-law decay, an asymptotic exponential decay occurs. Such asymptotic exponential decays were also observed when noise is included in open chaotic billiards [34]. The case with  $D \neq \gamma \neq 0$  (not shown here) was already studied recently [35] and the RTS mainly follows the behavior observed in Fig. 7(b). Thus, while noise may induce the asymptotic exponential decay observed in volume preserving systems, sinks generate the plateaus.

## VI. RTS IN A FLUID FLOW MODEL

For time-periodic 2D flows and steady 3D flows, regular and chaotic motions coexist and the increasing of mixing, resulting from the chaotic advection, is forbidden due the impenetrable barriers that separate the two distinct motions. However, for time-dependent 3D flows, complete uniform mixing is possible due to the *resonance-induced dispersion*, as mentioned in Sec. I. In this case an enhancement of diffusion in some regions of the space will occur [26]. The previous Sections showed the existence of these behaviors in the dynamics of the *ESM*, which lead us to conjecture that some aspects of the dynamics of a time-dependent 3D flow can be reproduced by a 3D volume preserving maps of the type action-action-angle.

In this Section we investigate the dynamics of a time-dependent non-Hamiltonian 3D flow model. We perform the RTS simulations for this model and compare the results with those described in Sec. IV A. The connection between RTS and transport in fluids is by itself an interesting problem [14]. The model used here is given by

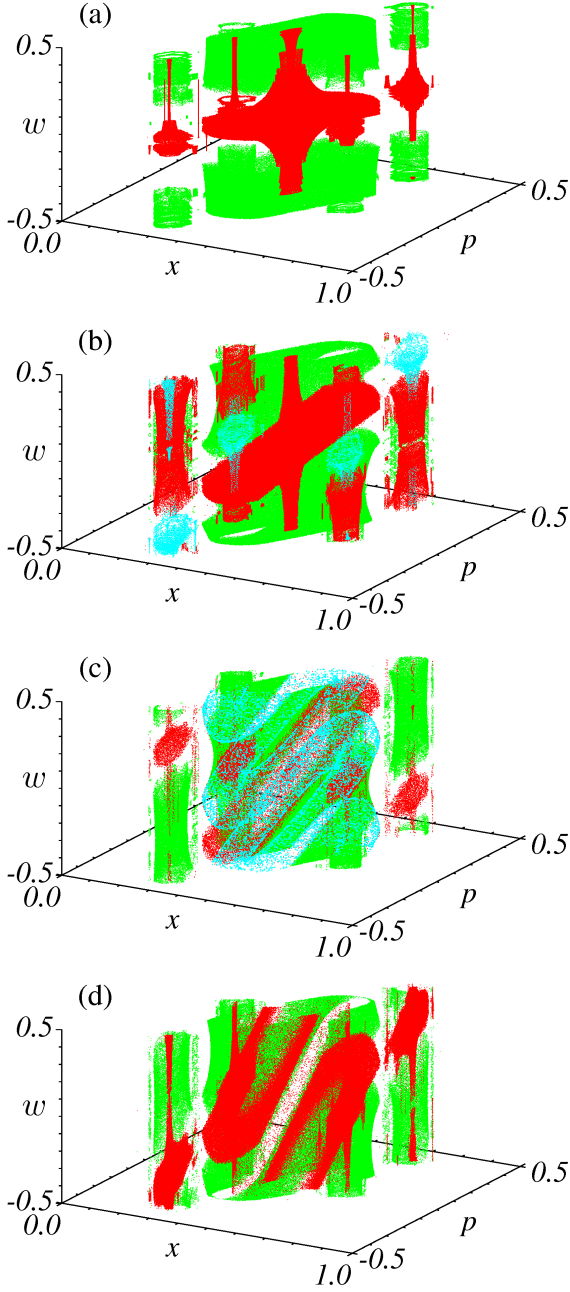


Figure 6. (Color online) Three-dimensional phase-space  $(x, p, w)$  for (a)  $K_2 = 0.09$  (regular dynamics); (b)  $K_2 = 2.6$  (mixed dynamics); (c)  $K_2 = 4.9$  (mixed dynamics) and (d)  $K_2 = 8.8$  (chaotic dynamics). These plots correspond respectively to Figs. 5 (a)-(d). Color denote the same time intervals from Fig. 5. For clarity the times  $\mathbf{O}_1$  (blue points) from Fig. 5 were not plotted.

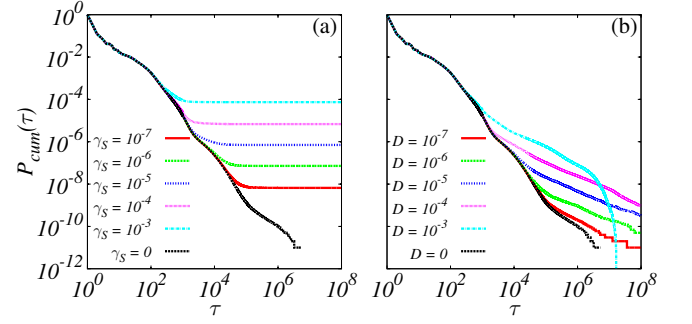


Figure 7. (Color online) Cumulative probability distributions for recurrence-times  $\tau$  for distinct values of (a) dissipation  $\gamma$  and (b) noise intensity  $D$ .

$$\begin{aligned} v_x &= -\cos(\pi x_s(t)) \sin(\pi y) + \epsilon \sin(2\pi x_s(t)) \sin(\pi z), \\ v_y &= \sin(\pi x_s(t)) \cos(\pi y) + \epsilon \sin(2\pi y) \sin(\pi z), \\ v_z &= 2\epsilon \cos(\pi z) [\cos(2\pi x_s(t)) + \cos(2\pi y)], \end{aligned} \quad (8)$$

where  $(x, y, z)$  and  $(v_x, v_y, v_z)$  represent respectively the fluid position and velocity. The explicit time dependence is given by  $x_s(t) = x + b \sin(\omega t)$ , where  $b$  and  $\omega$  are the non-dimensionalized oscillation amplitude and frequency, respectively. The coupling to the extra-dimension (secondary motion of the flow) is characterized by  $\epsilon$ . This model captures the essential features of an alternating vortex flow with Ekman pumping. For the two-dimensional uncoupled case  $\epsilon = 0$ , the motion is clearly separated in regular (vortices) and chaotic around the vortices. A tracer inside the chaotic region never crosses the regular region. However, tiny values of  $\epsilon$  are enough to induce a nearly uniform mixing. This mixing occurs via a spiraling motion (see [23] for more details).

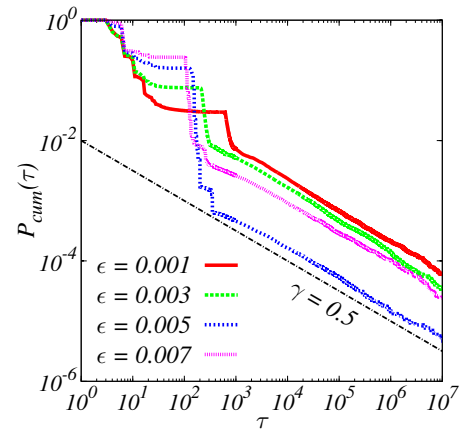


Figure 8. (Color online) Cumulative probability distributions for recurrence-times  $\tau$  for the flow described by Eq. (8) using  $b = 0.02$ ,  $\omega = 4.0$  and different values of coupling parameter  $\epsilon$ .



Figure 8 shows the RTS curves for the model (8). In our simulations we use fourth-order Runge-Kutta algorithm with fixed time-step  $\Delta t = 0.01$  for  $10^6$  recurrences. The similarities of these decays with Fig. 3(c),(g) and (k) are astonishing. The general sequence of decays is identical. Plateaus followed by an abrupt break and a very long random walk decay. The existence of plateaus is induced by the spiralling motion (trapping tube). After the abrupt break of the plateaus, particles from the fluid performs a random walk clearly characterized by the power-law  $P_{cum}(\tau) \propto \tau^{-0.5}$ . Thus the mixing process in the fluid dynamics is mainly governed by a random walk process. Trapping regime for short times, originating plateaus on the RTS curves as we found for the *ESM* in Fig. 3. Additionally, the influence of the parameter  $\epsilon$  can be compared to the parameter  $\delta$  for the *ESM*. By increasing the parameter the plateaus appear early and become shorter.

Another example of this behavior can be found in [22], as mentioned in Sec. I. For the model used by the authors, the interaction of the active particles with the fluid flow induces a complex behavior which cannot be reproduced by the individual systems. The dynamics of the fluid flow alone is composed of a chaotic sea and elliptic islands bounded by KAM tori that are impenetrable for the fluid elements. However, when it is coupled with the active particles dynamics, the swimmers can cross these boundaries. Transport decreases due to the formation of traps that can stuck the swimmers on nearly bounded orbits for long times [22], a feature similar to our observation in the *ESM* dynamics. Furthermore, some of these behaviors of flows and maps can also experimentally be observed for passive scalars in the Rayleigh-Benard system with oscillatory instability [25].

## VII. CONCLUSION

This work uses the RTS to describe the regular, mixed and chaotic dynamics in non-Hamiltonian 3D volume preserving systems. For this we use the standard map coupled to an extra-dimension and a continuous fluid flow model. The standard map is a typical system which allows us to make important general statements about the diffusion process steering the penetration of islands from the 2D case. In our case we do not have Arnold diffusion, but a process similar to the resonance-induced dispersion takes place [27, 28]. The general observed behavior for the decays of the RTS can be divided in two parts. Firstly, an initial exponential decay due to the chaotic regime **C**. This is a consequence of trajectories which do not touch the regular structure and are of no interest here. Second, the dynamics in the ordered regime **O**

(quase-regular motion), which is a consequence of particles which interact with the regular structure. This part contains power law decays due to sticky effects around the regular structure, plateaus due to trapping inside the regular structures (in this case a trapping tube or vortices in the fluid flow case), and asymptotic exponential decays. In addition to the above decays, when the mixed dynamics is considered in the extra-dimension, we also observe an abrupt break of the plateau due to a diffusive motion, followed by a random walk. The trapping times inside the regular structure are clearly recognized by the plateaus in the RTS and in the cumulative distribution of consecutive time spend inside the regime **O**. The large trapping times occur independent of the regular, mixed or chaotic dynamics of the extra-dimension and tends to infinity (but with decreasing probability to occur) for smaller and smaller couplings. The plateau time is shown to be inverse proportional to the coupling strength between the standard map and the extra-dimension. Compared to RTS in Hamiltonian systems, we observe that for mixed 3D volume-preserving systems the asymptotic exponential decays appear naturally (with one exception for  $K_2 = 4.9$ , but we believe this is a question of iteration times) and that plateaus seem to be a unique property of such 3D non-Hamiltonian conservative systems. Scaling properties show that the asymptotic behavior of decays and regimes is independent of the small coupling values. We also show that plateaus with infinite times appear when tiny dissipation is introduced in the standard map, and are consequences of the larger number of sinks. On the other hand, the standard map with a white noise is shown to induce an enhanced power-law decay followed by an asymptotic exponential decays with no plateaus.

The classification technique [30] of ordered and chaotic regimes allows us to show that all relevant dynamics occurs for the ordered regime, or quasi-regular dynamics. Asymptotic exponential decays of trajectories moving restricted to the boundaries of the islands from the uncoupled case suggest that the dynamics in this system belongs to the mixing one. Further interesting investigations is to use an extra-dimension for which the stable points remain stable. In such case the diffusion process is expected to differ from the observed here and it may change the asymptotic decay.

## ACKNOWLEDGMENTS

The authors thank FINEP (under project CTINFRA-1), C.M. and M.W.B. thank CNPq for financial support and M.W.B. thanks UDESC for the hospitality in November, 2014.

---

[1] H. Poincaré, Acta Math. **13**, 1 (1890).

[2] E. G. Altmann, A. E. Motter, and H. Kantz, Phys. Rev. E **73**, 026207 (2006).

- [3] D. L. Shepelyansky, Phys. Rev. E **82**, 055202 (2010).
- [4] E. G. Altmann, Ph.D. thesis, Max Planck Institut für Physik Komplexer Systeme (2007).
- [5] E. G. Altmann and A. Endler, Phys. Rev. Lett. **105**, 244102 (2010).
- [6] J. D. Bernal, J. M. Seoane, and M. A. F. Sanjuán, Phys. Rev. E **88**, 032914 (2013).
- [7] A. Kruscha, R. Ketzmerick, and H. Kantz, Phys. Rev. E **85**, 066210 (2012).
- [8] K. M. Frahm and D. L. Shepelyansky, Phys. Rev. E **85**, 016214 (2012).
- [9] V. S. Afraimovich, W. W. Lin, and N. F. Rulkov, Int. J. Bif. and Chaos **10**, 2323 (2000).
- [10] C. Manchein and M. W. Beims, Phys. Lett. A **377**, 789 (2013).
- [11] C. V. Abud and R. E. de Carvalho, Phys. Rev. E **88**, 042922 (2013).
- [12] E. G. Altmann and T. Tél, Phys. Rev. E **79**, 016204 (2009).
- [13] D. L. Vainchtein, A. I. Neishtadt, and I. Mezić, Chaos **16**, 043123 (2006).
- [14] G. M. Zaslavsky and M. K. Tippet, Phys. Rev. Lett **67**, 3251 (1991).
- [15] A. J. Lichtenberg and M. A. Lieberman, Regular and Chaotic Dynamics (Springer-Verlag, New York, 1992).
- [16] Y.-C. Lai and T. Tél, Transient Chaos (Springer-Verlag, New York, 2011).
- [17] J. M. Seoane and M. A. F. Sanjuán, Rep. Prog. Phys. **76**, 016001 (2013).
- [18] A. Ben-Mizrachi, I. Procaccia, and P. Grassberger, Phys. Rev. A **29**, 975 (1984).
- [19] E. Ott, Chaos in Dynamical Systems (Cambridge University Press, Cambridge, 2002).
- [20] T. Tél, G. Károlyi, A. Péntek, I. Scheuring, Z. Toroczkai, C. Grebogi, and J. Kadtke, Chaos **10**, 89 (2000).
- [21] P. Pramukul, A. Svenkeson, and P. Grigolini, Phys. Rev. E **89**, 022107 (2014).
- [22] N. Khurana, J. Blawdziewicz, and N. T. Ouellette, Phys. Rev. Lett. **106**, 198104 (2011).
- [23] T. H. Solomon and I. Mezić, Nature **425**, 376 (2003).
- [24] C. Torney and Z. Neufeld, Phys. Rev. Lett. **99**, 078101 (2007).
- [25] O. Piro and M. Feingold, Phys. Rev. Lett. **61**, 1799 (1988).
- [26] M. Feingold, L. P. Kadanoff, and O. Piro, J. Stat. Phys. **50**, 529 (1988).
- [27] J. H. E. Cartwright, M. Feingold, and O. Piro, Phys. Rev. Lett. **75**, 3669 (1995).
- [28] I. Mezić, Physica D **154**, 51 (2001).
- [29] A. Saichev and D. Sornette, Phys. Rev. E **87**, 022815 (2013).
- [30] R. M. da Silva, C. Manchein, M. W. Beims, and E. G. Altmann, Phys. Rev. E **91**, 062907 (2015).
- [31] J. Meiss, Chaos **25**, 097602 (2014).
- [32] Z. Levnajić and I. Mezić, Chaos **20**, 033114 (2010).
- [33] L. E. Reichl, The Transition to Chaos: Conservative Classical Systems and Quantum Manifestations (Springer, New York, 2004).
- [34] E. G. Altmann, J. C. Leitão, and J. V. Lopes, Chaos **22**, 026114 (2012).
- [35] C. S. Rodrigues, A. V. Chechkin, A. P. S. de Moura, C. Grebogi, and R. Klages, Europhys. Lett. **108**, 40002 (2014).